CHEMICAL GENETICS ANALYSIS OF AN ANILINE MUSTARD ANTICANCER AGENT REVEALS COMPLEX I OF THE ELECTRON TRANSPORT CHAIN AS A TARGET*

Bogdan I. Fedeles[1], Angela Y. Zhu[1], Kellie S. Young[1], Shawn M. Hillier[1§], Kyle D. Proffitt[1‡], John M. Essigmann[1] and Robert G. Croy[1]

From Department of Biological Engineering and Department of Chemistry, Massachusetts Institute of Technology, Cambridge, MA, 02139, USA[1]

Running head: Antitumor agent induces ROS and inhibits complex I

Address correspondence to: Robert G. Croy and John M. Essigmann, Bldg. 56 Rm. 669, Massachusetts Institute of Technology, 77 Massachusetts Ave, Cambridge, MA 02139; Fax: 617-253-5445; Email: rgcroy@mit.edu and jessig@mit.edu

The antitumor agent 11β (CAS # 865070-37-7), consisting of a DNA damaging aniline mustard linked to an androgen receptor (AR) ligand, is known to form covalent DNA adducts and to induce apoptosis potently in AR-positive prostate cancer cells *in vitro*; it also strongly prevents growth of LNCaP xenografts in mice. The present study describes the unexpectedly strong activity of 11β against the AR-negative HeLa cells, both in cell culture and tumor xenografts, and uncovers a new mechanism of action that likely explains this activity. Cellular fractionation experiments indicated that mitochondria are the major intracellular sink for 11β; flow cytometry studies showed that 11β exposure rapidly induced oxidative stress, mitochondria being an important source of reactive oxygen species (ROS). Additionally, 11β inhibited oxygen consumption both in intact HeLa cells and in isolated mitochondria. Specifically, 11β blocked uncoupled oxygen consumption when mitochondria were incubated with complex I substrates, but it had no effect on oxygen consumption driven by substrates acting downstream of complex I in the mitochondrial electron transport chain. Moreover, 11β enhanced ROS generation in isolated mitochondria, suggesting that complex I inhibition is responsible for ROS production. At the cellular level, the presence of antioxidants (N-acetylcysteine or vitamin E) significantly reduced the toxicity of 11β, implicating ROS production as an important contributor to cytotoxicity. Collectively, our findings establish complex I inhibition and ROS generation as a new mechanism of action for 11β, which supplements conventional DNA adduct formation to promote cancer cell death.

Adaptive responses to hypoxia and oxidative stress allow tumor cells to exist and grow under adverse conditions and to acquire therapeutic resistance, contributing to the failure of chemotherapy for prostate and other cancers (1). Strategies to overcome resistance include development of agents with multiple cytotoxic mechanisms; such strategies could include a primary toxicity mechanism (e.g., DNA damage) that is complemented by a secondary stressor, such as the intentional generation of oxidative stress or the inhibition of natural antioxidant enzymes (2). In fact, many clinically useful drugs have more than one mechanism of toxicity. Reactive oxygen species (ROS) have been implicated to varying extents in the cytotoxic mechanisms of cisplatin (3), doxorubicin (4), bleomycin (5) and etoposide (6). It is thought that ROS may be supplementing the primary mechanism of toxicity of each of these agents.

The small-molecule anticancer agent 11β (Fig. 1A) was designed to kill androgen receptor (AR) positive prostate cancer cells by targeting both DNA replication (via its aniline mustard moiety, which forms DNA adducts) and the expression of steroid-responsive genes (via its steroid ligand). The structure of 11β features the DNA-reactive p-*N,N*-bis-(2-chloroethly)aminophenyl group linked to an estradien-3-one ligand (Fig. 1A), which has a high affinity for the AR (7). It was originally proposed that the DNA adducts formed by 11β could bind the AR and potentially disrupt tumor cell biology by two non-mutually exclusive mechanisms: (i) antagonism of AR-regulated gene expression, and (ii) obstruction of the DNA repair process. Recent studies demonstrate that 11β induces apoptosis in AR+ prostate cancer cells, is stable *in vivo*, and effectively prevents the growth of AR+ LNCaP tumors as xenografts in mice (7;8). While very effective against AR+ cells and

tumors, 11β has surprisingly potent activity against AR- cells and tumors, leading to reconsideration of the role of the AR in the process leading to cell death. The present study is the result of the search for AR-independent mechanisms of 11β toxicity.

Previous studies (7) revealed that 11β induces apoptosis at lower exposure levels and much more rapidly than DNA damaging aniline mustard drugs such as chlorambucil (Fig. 1), which contains the same alkylating group. Within 6 h of treatment with >5 μM 11β, LNCaP cells undergo cytoplasmic contraction and detachment from the culture dish, while treatment with similar or even higher concentrations of chlorambucil has little effect on cell morphology and does not induce apoptosis (7). In addition, 11β-dim, a DNA-unreactive analog of 11β (Fig. 1), produces similar morphological changes but does not induce apoptosis in the same concentration range (7), further suggesting the possibility of additional mechanisms of cytotoxicity.

The current study demonstrated that 11β potently induced apoptosis in AR-negative HeLa cells both *in vitro* and when grown as xenograft tumors in mice. Furthermore, both 11β and its analog, 11β-dim (Fig. 1), generated a burst of intracellular ROS, whereas in the same dose ranges, chlorambucil or the steroid moiety of 11β alone (estradien-3-one) did not. The functional role of ROS was evidenced by co-treatment with antioxidants, which reduced ROS formation and suppressed the cytotoxicity of both 11β and 11β-dim. Additional experiments indicated that mitochondria were the main intracellular sink for 11β and an important source of the ROS, which were produced due to the specific inhibition of complex I of the mitochondrial electron transport chain (ETC). Together, these findings established ROS production and complex I inhibition as new, DNA adduct independent mechanisms of 11β that supplemented the compound's ability to kill tumor cells by covalent DNA damage. The data also suggested that 11β could be active against a wide range of tumors, including those that do not express the AR and added support the growing body of evidence that oxidative stress may synergize with conventional DNA adducts to promote cancer cell death.

EXPERIMENTAL PROCEDURES

Reagents- The compounds 11β and 11β-dim were synthesized as previously reported (7). ^{14}C-11β was prepared as described in (8). Stock solutions of test compounds were prepared in DMSO and stored at -80°C. All chemical reagents were purchased from Sigma-Aldrich (St.Louis, MO, USA), unless indicated otherwise. 17β-Hydroxy-estra-4(5),9(10)dien-3-one (estradien-3-one) was obtained from Brighton Co. LTD, Chang Sha, Hunan, China. CM-H_2DCFDA, CM-DCFDA, MitoSOX and JC-1 molecular dyes were obtained from Molecular Probes (Invitrogen, Carlsbad, CA, USA). All cell media, media supplements, DPBS and HBSS were from Invitrogen. CTB reagent was purchased from Promega (Madison, WI, USA).

Cell lines and culture- HeLa cells were obtained from American Type Culture Collection (Rockville, MD, USA) and maintained in Minimal Essential Medium (MEM) supplemented with 1 mM glutamax, 1% non-essential amino acids, 1 mM pyruvate, and 10% fetal bovine serum (Hyclone, Logan, UT, USA), in a humidified 5% CO_2/air atmosphere at 37°C.

Determination of cytotoxicity and cell viability- Clonogenic survival assays were performed by seeding 1×10^3 HeLa cells per well in 6-well plates, followed by growth for 24 h to allow cell attachment. Test compounds dissolved in DMSO were added to growth media for 24 h, replaced with fresh medium and growth continued for 3-5 days until colonies were clearly visible. Colonies were fixed with water:methanol:acetic acid (4:5:1), stained 0.5% crystal violet and manually counted. The surviving fraction was calculated as the ratio of the number of colonies in treated well to the number in untreated wells. Cell viability was estimated using the Cell-Titer Blue (CTB) assay as described in the manufacturer's instructions. Briefly, 2.5×10^3 cells/well were seeded in black/clear bottom 96-well plates (Corning Inc., Corning, NY, USA) and incubated for 24 h. Media was then replaced with fresh drug-containing media for the indicated times. CTB reagent was then added for 2-4 h after which fluorescence (ex/em: 555/585 nm) was measured. Cell viability was calculated as the ratio between the average background corrected signal in the treated wells and the untreated control wells.

Immunoblot analysis- Whole cell extracts of HeLa cells were prepared by lysis in RIPA solution according to manufacturer's instructions (Santa Cruz Biotechnology, Santa Cruz, CA, USA). Equal amounts of protein were separated by SDS-PAGE and transferred to Immobilon-P membranes (Millipore, Bedford, MA, USA). Membranes were probed with primary antibodies anti-caspase-3 (#9665), anti-caspase-9 (#9502), anti-PARP (# 9542) and secondary antibody anti-rabbit IgG-HRP (#7074); all antibodies were from Cell Signaling Technology (Danvers, MA, USA). Detection of antibody complexes was achieved by PicoWest chemoluminescence reagent (Pierce, Rockford, IL, USA).

Determination of intracellular ROS using flow cytometry- Intracellular ROS levels were measured with fluorometric dyes. 1×10^5 HeLa cells were seeded in 6-well plates and grown for 24 hours. After the cells were exposed to test compounds for the indicated times, the cells were washed with PBS and exposed to a molecular probe solution in HBSS at 37°C. The molecular probes and their final concentrations were: CM-H_2DCFDA (2.5 μM), CM-DCFDA (2.5 μM) and MitoSOX (2 μM). After incubation for 15 min at 37°C, the cells were washed, trypsinized, resuspended in HBSS and analyzed on the FL1 channel (CM-H_2DCFDA, CM-DCFDA) or the FL2 channel (MitoSOX) of a Becton Dickinson FACSCanto II flow cytometer. The results were analyzed with FACSDiva 6.0 software (BD, Franklin Lakes, NJ, USA).

Determination of mitochondrial membrane potential- Mitochondrial inner membrane potential ($\Delta\Psi m$) was estimated using the mitochondrial-specific dye JC-1 according to a published flow cytometry protocol (9). Briefly, after treatment, cells were incubated at 37°C with a solution of JC-1 in medium without phenol red for 30 min, then trypsinized, resuspended in PBS and analyzed on a FACSCanto II flow cytometer. The mitochondrial membrane potential was estimated by the ratio between the red (FL2) and green (FL1) fluorescence. The results were analyzed with FACSDiva 6.0 software (BD).

Determination of H_2O_2, lipid peroxidation and NADPH- Cellular levels of H_2O_2 were measured using the Quantichrom Peroxide Assay (Bioassay Systems, Hayward, CA, USA) according to the manufacturer's instructions. Lipid peroxidation was monitored using the OxiSelect TBARS assay (Cell Biolabs, Inc., San Diego, CA, USA) as described in the manufacturer's instructions. Cellular NADPH content was measured using the EnzyChrom NADP/NADPH assay (BioAssay Systems) according to the manufacturer's instructions. In all assays, the results were normalized for protein content, determined using the Bradford reagent (Bio-Rad, Hercules, CA, USA).

Fluorescence microscopy- Cells were grown on poly-lysine coated coverslips, in 6-well plates. The seeding and treatment with test compounds was performed identically to the viability assay. After treatment, the cells were stained for 10 min at 37 °C with 1 μM MitoSOX and 5 μM Hoechst 33342 in HBSS, washed 3 times in fresh HBSS and imaged with a Nikon Eclipse fluorescence microscope.

Cell fractionation and mitochondria isolation- The protocol was adapted from reference (10) with modifications. All steps were performed at 4°C. 3×10^7 HeLa cells were detached by scraping, washed in cold DPBS and resuspended in 3 mL isolation buffer (Buffer IB: 10 mM Tris-MOPS, 1 mM EGTA-Tris, 200 mM sucrose, pH = 7.4). The cells were disrupted with a tight-fitting Dounce homogenizer, on ice (30 strokes). The homogenate was sedimented at 800 × g for 10 min to yield a nuclear pellet. The supernatant was further sedimented at 8000 × g for 10 min to yield the mitochondrial pellet. Finally, the post-mitochondrial supernatant was centrifuged at 100,000 × g (Beckmann Ultracentrifuge) for 1 h to separate the microsomal fraction (pellet) from the cytosol (supernatant). For oxygen consumption studies, rat liver mitochondria were isolated using a similar protocol (10). Mitochondria isolated from fresh rat liver were kept on ice and used the same day. Total mitochondrial protein was determined by hydrolyzing mitochondrial aliquots in NaOH, 0.5 M and then using the Bradford method.

Cellular localization of 11β- To determine the cellular distribution of 11β, HeLa cells were treated with ^{14}C-11β for 6 h, then subjected to fractionation. Aliquots of each fraction were suspended in scintillation fluid (EcoScint H) and radioactivity was measured using a Beckmann LS 6500 scintillation counter.

Oxygen consumption– Oxygen consumption was measured with a PreSens Fibox 3 (Precision Sensing, Regensburg, Germany) oxygen mini-sensor, according to manufacturer's instructions. All measurements were done at room temperature. For cellular oxygen consumptions, HeLa cells were washed, trypsinized and resuspended in cell culture medium at 5×10^6 cells/mL. Mitochondrial oxygen consumption was measured as described (10) using the substrates: 5mM glutamate/2.5 mM malate (complex I) or 5 mM succinate (complex II) or 6 mM ascorbate/300 μM TMPD (cytochrome c/complex IV). Mitochondria were suspended in experimental buffer (Buffer EB: 12.5 mM KCl, 10 mM Tris-MOPS, 0.1 mM EGTA-Tris, 1 mM KH_2PO_4, pH 7.4), at a concentration of 2 mg/mL of mitochondrial protein. To measure NADH driven oxygen consumption, mitochondria were permeabilized to NADH using three freeze-thaw cycles.

ROS measurement in isolated mitochondria– Rat liver mitochondria (0.5 mg/mL protein concentration) were incubated at 37 °C in EB, supplemented with 0.1% BSA, 5 mM glutamate, 2.5 mM malate, 0.05 U/mL horseradish peroxidase (HRP) and 10 μM Amplex Red reagent, in the presence of DMSO (control) or test compound, with or without 2000 U/mL of bovine liver catalase (Roche, Indianapolis, IN, USA). After 20 minutes in the dark, the fluorescence of the resorufin generated by Amplex Red was monitored for 20 minutes in a SpectraMax M3 spectrophotometer (Molecular Devices, Sunnyvale, CA, USA). The amount of H_2O_2 generated was calculated from a H_2O_2 standard curve obtained in similar conditions.

Complex I activity assay– Complex I activity was measured by using the synthetic electron acceptor decylubiquinone (Sigma) and monitoring the rate of NADH disappearance (11). Rat liver mitochondria were permeabilized to NADH with 3 freeze-thaw cycles, diluted to 0.25 mg/mL (total mitochondrial protein) in potassium phosphate buffer (25 mM, pH 7.4) and supplemented with 0.35% BSA, 1 μM antimycin, 1 mM KCN and 70 μM decylubiquinone. NADH (0.1 mM) and the test compound (or DMSO control) were added last. After a brief and thorough mixing, the drop in the absorbance difference A_{340}-A_{380} was monitored in a quartz cuvette on a Beckmann Coulter DU730 Spectrophotometer at room temperature. Complex I activity was then calculated using ε_{NADH} for A_{340}-A_{380} as 5.5 mM^{-1} cm^{-1} (11).

Tumor xenograft studies and immuno-histochemistry- HeLa cells (6×10^6) suspended in 50% PBS/50% Matrigel (BD) were injected subcutaneously in the right flank of 6-week old NIH Swiss nu/nu female mice. Mice developing subcutaneous tumors within 2 weeks were randomized to treatment and control groups. Administration of test compound dissolved in cremophore EL, saline, ethanol (43:30:27) was begun when established tumors reached approximately 7 mm diameter. Tumor measurements obtained with vernier calipers and tumor volumes estimated using the formula ($width^2 \times length \times 3.14$)/6. Experiments were carried out under the guidelines of the MIT Animal Care Committee.

Statistical analysis- All results are expressed as mean ± standard deviation. The significance of the difference between two populations was calculated using Student's two-tailed t-test for unpaired data sets with unequal variances. P-Values less than 0.05 were considered significant. The LC_{50} and EC_{50} values were calculated from the dose response curves by using 4 variable logistic curve fitting function in Prism 3.0 for Windows (GraphPad Software Inc., San Diego, CA, USA).

RESULTS

The toxicity of 11β towards HeLa cells. Our investigations sought to uncover mechanisms of toxicity that were unrelated to the affinity of 11β for the AR. HeLa cells, which do not express the AR (12), were chosen to assess the respective contributions of the steroid and alkylating portions of the compound (Fig. 1). Chlorambucil was used as a model of the reactive alkylating portion of 11β since both molecules share the p-*N,N*-bis-(2-chloroethyl)aminophenyl group that can form a reactive aziridine capable of covalent modification of DNA and other cellular molecules. To investigate the non-covalent interactions of 11β, an analog, 11β-dim (Fig. 1A) was prepared. This compound was unreactive towards the model nucleophile 4-(4-nitro-benzyl)-pyridine (NBP) (Supplemental data, Fig. S1), indicating that it lacked the ability to modify DNA covalently. It was thus expected that any observed 11β-dim

toxicity would arise only from non-covalent interactions with cellular targets.

Cell viability analysis, performed using the CellTiter Blue (CTB) assay (Fig. 1B), revealed a steep dose response to concentrations of 11β >5 μM, and a similar steep response observed at higher concentrations (>12 μM) with 11β-dim. By contrast, neither chlorambucil nor estradiene-3-one at 20 μM decreased the CTB signal by more than 25% (Fig. 1B). Both 11β and 11β-dim exhibited a threshold effect above which cell viability rapidly decreased; such an effect was not observed with either chlorambucil or estradiene-3-one.

Given the striking decrease in viability that was observed after a 24 h treatment with 11β, it was of interest to determine the effect of shorter exposure times on cell viability. HeLa cells were exposed to increasing concentrations of 11β for 3, 6 or 24 h and cell viability was measured at 24 h. Comparable toxicities were achieved for 6 or 24 h exposures to 11β (6 h, EC_{50} = 5.3 ± 0.3 μM; 24 h, EC_{50} = 4.9 ± 0.3 μM), while a 3 h exposure period resulted in lower levels of toxicity (Fig. 1C). Together, these data suggested that a 6 h exposure was sufficient for achieving maximum toxicity of 11β for most doses. Therefore, subsequent mechanistic experiments focused on cellular changes that occur during the initial 6 h.

Activation of apoptotic pathways by 11β was previously observed in LNCaP cells (7). To determine whether apoptosis was also the mechanism of cell death in HeLa cells, the proteolytic cleavage of caspase-9, caspase-3 and poly-ADP ribose polymerase (PARP) were investigated. Western analysis with corresponding antibodies revealed that a 6 h treatment with 7.5 μM or 10 μM 11β induced cleavage of caspase-9, caspase-3 and PARP (Fig. 1D).

11β accumulates in the mitochondria. To understand better the putative targets of 11β, an intracellular localization study was performed. HeLa cells were treated with 5 μM ^{14}C-labeled 11β for 6 h, isolated and subjected to subcellular fractionation (see Materials and Methods). By measuring the radioactivity associated with the medium and the cell pellet, it was found that a significant portion of the total compound (over 30%) becomes associated with the cells in 6 h (Fig. 2A). Subcellular fractionation revealed that 50 ± 2% of the radioactive compound is found in the mitochondrial fraction, while the rest is distributed among the nucleus, microsomes and cytosol (Fig. 2B). The radioactivity measurements also allowed the estimation of the local concentration of 11β (Fig. 2C), the compound being most concentrated in the mitochondria (9.9 ± 0.4 pmol/μg protein) and the microsomes (8.5 ± 0.5 pmol/μg protein). By assuming the volume of a HeLa cell of 4.2 pL (measured average diameter = 20 μm), the molar concentration of 11β in the cell after 6 h was estimated to be ~300 μM, a 60 fold increase from the 5 μM concentration in the medium. Moreover, using the published value for the mitochondrial volume of 1.6 μL/mg mitochondrial protein (13), the molar concentration of 11β in the mitochondria was estimated to be ~6 mM , which is more than 1000 fold increase from the medium concentration of 11β. These findings suggest that mitochondria might be one of the targets of the compound.

11β increases intracellular ROS. The observation that the DNA-unreactive 11β-dim is nevertheless toxic (Fig. 1B) indicated that 11β may be employing several mechanisms of toxicity. Given the rapid activation of the apoptotic pathway (Fig. 1C) and the mitochondrial localization of 11β (Fig. 2B), we hypothesized that one such mechanism may involve direct mitochondrial toxicity.

One of the hallmarks of mitochondrial dysregulation is the generation of ROS and oxidative stress (14;15). Generation of ROS in HeLa cells was monitored using the molecular probe CM-H_2DCFDA, which can detect most ROS at a cellular level (16). Once inside a cell, this probe is de-acetylated by cellular esterases and, when oxidized, it becomes the fluorescent compound CM-DCF, which can be detected in the FL1 channel of a flow cytometer. Fig. 3A is a fluorescence histogram showing that treatment of HeLa cells for 6 h with 3 or 5 μM 11β resulted in a notable increase in CM-DCF fluorescence intensity (right shift) compared to DMSO (vehicle) treated cells. The possibility that increased fluorescence was due to increased uptake of the probe was ruled out by use of a related molecular probe, CM-DCFDA, which does not require oxidation to become fluorescent. When using CM-DCFDA, no significant increase in CM-DCF fluorescence was detected in the treated cells compared to controls, indicating that cellular

uptake of the dye was unaffected by 11β. These findings together established that 11β treatment triggered a significant production of ROS.

To determine whether the production of ROS required the ability of 11β to modify cellular molecules covalently, ROS levels were compared between cells treated for 6 h with 11β (5 μM) , 11β-dim (10 μM), chlorambucil (10 μM) or estradien-3-one (10 μM) (Fig. 3B); antimycin A, a known ROS inducer, was included as a comparative control. The data revealed that both 11β compounds were potent inducers of ROS, while chlorambucil and estradien-3-one were not. Several other doses of each compound were investigated, revealing a dose-response dependence for 11β and 11β-dim (Supplemental data, Fig. S2). Thus, neither the ability to form covalent adducts (characteristic of 11β and chlorambucil), nor the presence of the steroid group (11β, 11β-dim and estradien-3-one) correlates with the ability to induce ROS. The operative structural feature responsible for the ROS induction appears to be the entire molecular framework of 11β or 11β-dim.

To investigate the kinetics of intracellular ROS generation, a time course of ROS levels was measured in HeLa cells treated with 5 μM 11β. Increased levels of ROS were detected as early as 30 min after addition of 11β to culture media and then the levels continued to increase in the first 6 h of exposure (Fig. 3C), suggesting that 11β caused both rapid-onset and sustained ROS generation. Several markers of oxidative stress in 11β-treated cells were also increased, including levels of hydrogen peroxide (Fig. 3D) and the secondary oxidation product, malondialdehyde (Fig. 3E). Additionally, the cellular levels of NADPH, the principal cellular reducing co-factor, decreased rapidly during the same time interval (Fig. 3F). These findings are consistent with the rapid formation of ROS in HeLa cells exposed to 11β suggesting that ROS and generalized oxidative stress may contribute to 11β cytotoxicity.

Antioxidants decrease ROS levels and reduce 11β toxicity. To establish a link between ROS production and the toxicity of 11β, HeLa cells were treated with 11β in the presence of antioxidants. A significantly lower level of ROS (p<0.01) was observed when HeLa cells were exposed to 5 μM 11β for 6 h in the presence of antioxidants N-acetyl-L-cysteine NAC (10 mM) or vitamin E (100 μM) (Fig. 4A). Additionally, both NAC and vitamin E reduced the toxic effect of 11β on cell viability, measured with the CTB assay. The EC_{50} for 11β increased significantly from 4.9 ± 0.3 μM to 6.9 ± 0.7 μM in the presence of NAC and to 7.5 ± 0.1 μM in the presence of vitamin E (Fig. 4B). Antioxidants also attenuated the adverse effect of 11β-dim on cell viability; the EC_{50} increased from 13.7 ± 0.3 μM to > 20 μM in the presence of NAC or vitamin E (Fig. 4C).

Mitochondrial superoxide generation and increased ΔΨm in 11β-treated cells. Mitochondrial ROS production was monitored with MitoSOX Red, a cationic dye that localizes in the mitochondria and specifically reacts with superoxide ($O_2^{\bullet-}$). The product of this reaction (a 2-hydroxyethidium derivative) can then be detected by fluorescence microscopy or FACS (17). HeLa cells treated with 5 μM 11β for 6 h showed increased MitoSOX fluorescence (Fig. 5A), signaling the exaggerated production of $O_2^{\bullet-}$ by mitochondria. A dose-response relationship revealed that concentrations of 11β >5 μM resulted in a significant $O_2^{\bullet-}$ production (Fig. 5B).

To analyze further the effects of 11β on mitochondria, changes in the mitochondrial inner membrane potential (ΔΨm) were measured with the ΔΨm indicator JC-1. At 6 h, even low concentrations of 11β (< 5 μM) produced a significant increase in ΔΨm (Fig. 5C), indicating a hyperpolarization of the mitochondrial inner membrane. A higher-than-normal ΔΨm suggests a stalled mitochondrial ETC, which leads to a higher electron density in the upstream mitochondrial carriers and an increased likelihood of stray electron transfer to O_2 to generate superoxide (18). To investigate further this sequence of events, ΔΨm was measured in cells treated with 5 μM 11β in the presence of the antioxidants NAC and vitamin E. Although co-treatment with antioxidants leads to lower cellular ROS levels (Fig. 4A), it does not affect the increase in ΔΨm triggered by 11β (Fig. 5C). This finding suggests that the changes in the mitochondrial membrane precede ROS generation, and further establishes mitochondria as one of the targets of 11β.

Effect of 11β on mitochondrial respiration. The perturbation of ΔΨm and the increased formation of mitochondrial superoxide suggested that 11β could act as an inhibitor of mitochondrial

respiration, by interfering with the ETC. To test this hypothesis, the cellular oxygen consumption was measured first in intact HeLa cells. The cells were exposed to 5 μM 11β or DMSO control for 3 h, then the oxygen consumption was measured using a Fibox 3 oxygen sensor, in the presence of 1 nM FCCP (a potent uncoupler of mitochondrial oxidative phosphorylation). By using the uncoupler, the oxygen consumption measured reflected only the flow of the electrons through the ETC, irrespective of the energetic state (ATP levels) of the cell. The results indicated that cells treated with 11β had a 26 ± 7% lower respiration rate than untreated cells (Fig. 6A).

To confirm the suppressive effect on cellular respiration, oxygen consumption was measured in isolated rat liver mitochondria, in the presence of various respiratory substrates. When mitochondria, uncoupled with 1 nM FCCP, were incubated with complex I substrates glutamate and malate, both 11β and 11β-dim significantly (p<0.01) reduced the rate of oxygen consumption (Fig. 6B). Specifically, 10 μM of either compound caused a 70 ± 5% decrease in respiration rate. In the same conditions, the potent complex I inhibitor, rotenone (1 μM) caused a 92 ± 5% decrease in respiration rate. However, when mitochondria were incubated with succinate, a complex II substrate, in the presence of rotenone (to block complex I activity), neither 11β or 11β-dim had any significant effect on the respiration rate (Fig. 7B). Additional experiments, utilizing ascorbate and N,N,N',N'-tetramethyl-p-phenylenediamine (TMPD), which are commonly used substrates to feed electrons into the ETC at the level of cytochrome c, downstream of complex III (10), showed no inhibition of oxygen consumption by 11β or 11β-dim (data not shown). Together, these observations suggest that the main target of the 11β compounds in the ETC is complex I.

11β is an inhibitor of the mitochondrial NADH dehydrogenase (complex I). To confirm the hypothesis that 11β inhibits mitochondrial complex I, oxygen consumption of isolated mitochondria was measured using NADH as a substrate. Because NADH cannot freely diffuse through mitochondrial membranes, mitochondria were first permeabilized with three freeze-thaw cycles, and then oxygen consumption rate was measured as above. Both 11β and 11β-dim inhibited NADH-driven mitochondrial respiration (Fig. 6C). In these conditions, the 11β compounds achieved inhibition levels comparable to those of rotenone. To validate this result further, the effect of 11β on complex I was assessed using a direct mitochondrial NADH dehydrogenase assay. This assay utilizes permeabilized mitochondria and measures the oxidation rate of NADH in the presence of decylubiquinone, a synthetic electron acceptor specific to complex I (see Materials and Methods). Doses of 5 and 10 μM 11β significantly inhibited the oxidation rate of NADH (Fig. 6D). Taken together, these data established complex I as the direct target of 11β in the mitochondria.

Generation of ROS in isolated mitochondria. The relationship between complex I inhibition and ROS production was also examined in isolated mitochondria. Intact rat liver mitochondria, charged with complex I substrates glutamate and malate, were incubated with DMSO control, 11β, 11β-dim or rotenone, in the presence or absence of 2000 U/mL of catalase. After 20 min, the Amplex Red reagent was added to quantitate the rate of H_2O_2 generation. Both 11β compounds increased significantly (p <0.01) the rate of H_2O_2 production in isolated mitochondria (Fig. 6E). The increase in rate (22 ± 6% for 10 μM 11β) was comparable to that caused by rotenone (1 μM), a known ROS inducer and mitochondrial toxin. Additionally, in the presence of catalase, an enzyme that breaks down H_2O_2, no significant increase was observed (Fig. 6E), suggesting that H_2O_2, resulting presumably from the dismutation of superoxide, was the main ROS diffusing out of the mitochondria in the presence of 11β.

Toxicity of mixtures of 11β-dim and chlorambucil. While both 11β and 11β-dim induce ROS and have similar inhibitory effects on the mitochondrial ETC, 11β is more toxic (Fig. 1B). In a clonogenic survival assay (Fig. 7), 11β (LC_{50} = 1.7 ± 0.1 μM) had much greater toxicity toward HeLa cells than either 11β-dim (LC_{50} = 8.1 ± 0.1 μM) or chlorambucil (LC_{50} > 10 μM). To test whether the combination of ROS and the covalent modification of cellular molecules was responsible for 11β's increased cytotoxicity, a clonogenic survival assay was performed with HeLa cells treated with equimolar mixtures of chlorambucil and 11β-dim. The equimolar mixture of the two compounds had a greater toxicity (LC_{50} = 6.3 ± 0.1 μM) than either compound alone (Fig. 7). In fact, the LC_{50} value was nearly identical to the

theoretical value corresponding to the linear addition of toxicities of the two compounds. However, the toxicity of the equimolar mixture did not reach the potency of 11β itself (LC_{50} = 1.7 ± 0.1 μM), suggesting that the two mechanisms of toxicity synergize only when the molecular feature responsible for ROS and the feature responsible for covalent DNA adduct formation are present in the same molecular structure.

Effects of 11β treatment on HeLa mouse xenograft tumors. A previous report demonstrated that 11β is very effective in preventing the growth of LNCaP (AR+) prostate cancer cell xenografts in nude mice (7). The remarkable toxicity of 11β against HeLa cells (an AR- cell line) in cell culture predicted that the compound could be active against AR-independent tumors. Accordingly, mice bearing HeLa tumor xenografts were treated with three consecutive weekly 5-day cycles with a daily dose of 30 mg/kg (i.p.), while control animals received vehicle only. This treatment regimen produced a strong inhibition of tumor growth in the mice that received 11β (Fig. 8).

DISCUSSION

11β was designed to act by producing covalent DNA adducts that form complexes with the AR. In accord with predictions, 11β rapidly induces apoptosis in the AR-positive LNCaP cells (7). It is shown here that HeLa cells, which do not express the AR, are also rapidly killed by 11β, suggesting additional, AR-independent mechanism(s) of action. This study demonstrates that 11β unexpectedly accumulates in the mitochondria and inhibits the mitochondrial ETC at complex I, leading to an overproduction of ROS and oxidative stress. The direct mitochondrial toxicity and the production of ROS are novel toxicological supplements to the original design features of 11β.

11β was found to cause a rapid increase in the intracellular levels of ROS and biomarkers of oxidative stress (Fig. 3). Evidence of the involvement of ROS in 11β toxicity was provided by the abilities of the antioxidants NAC and vitamin E to lower the amounts of intracellular ROS (Fig. 4A) and increase cell viability (Fig. 4B). The overproduction of ROS in 11β-treated HeLa cells was not dependent on the ability of the compound to form DNA adducts, as evidenced by the observation of comparable levels of ROS in cells treated with 11β or the DNA-unreactive analog 11β-dim (Fig. 3B). Furthermore, no significant ROS production was detected in cells treated with either estradien-3-one (the steroid moiety of 11β) or chlorambucil (the alkylating moiety), suggesting that the entire molecular scaffold of 11β or 11β-dim was responsible for inducing ROS production. It is noteworthy that the 11β-dim compound was less toxic than 11β, indicating that the alkylating functionality also makes a significant contribution to toxicity.

The mechanism by which 11β stimulates the increased production of ROS appears to be the inhibition of mitochondrial ETC due to the direct inhibition of the NADH dehydrogenase (complex I). A number of experimental observations support this view. Firstly, subcellular localization studies showed that 11β accumulates in the mitochondria of HeLa cells. This observation is consistent with the biophysical properties of the 11β molecule, which is both highly hydrophobic (logP value ~5), and positively charged (the secondary amine functionality in the linker is predominantly protonated at physiological pH). Many lipophilic cations, such as cationic aromatic dyes and triphenyl phosphonium conjugates are known to accumulate in mitochondria (19;20). Secondly, 11β disrupted inner mitochondrial membrane potential (Fig. 5C) and cellular respiration (Fig. 6A), observations consistent with mitochondrial toxicity. Even a non specific accumulation of 11β within the mitochondrial membrane could disrupt the flow of electrons through ETC leading to increased $\Delta\Psi m$, which in turn could lead to increased ROS production (18;21). Thirdly, experiments with isolated mitochondria indicated that 11β inhibited mitochondrial respiration specifically at complex I (Fig. 6B, 6C). When mitochondria were incubated with substrates that feed electrons into the ETC downstream of complex I, no inhibition was observed (Fig. 6B). Further experiments confirmed the inhibitory effect of 11β on the NADH dehydrogenase (complex I) (Fig. 6C, 6D). Finally, complex I inhibition by 11β was shown to be sufficient to increase the rate of production of H_2O_2 in isolated mitochondria (Fig. 6E), providing a mechanistic explanation for the increased mitochondrial superoxide production (Fig. 5A) and general oxidative stress observed in cells treated with 11β (Fig. 3). These observations are in

good agreement with the currently accepted model of mitochondrial ROS production being due to ETC stalling and electron leakage from complexes I and III (21). These stray electrons incompletely reduce molecular oxygen to generate superoxide, an ROS confined to the mitochondria due to its charge. The activity of the mitochondrial superoxide dismutase then converts superoxide into oxygen and hydrogen peroxide, the latter being able to diffuse out of the mitochondria (21).

Mitochondrial toxicity leading to oxidative stress is a known cytotoxic mechanism for other compounds with clinical relevance. For example, the cytotoxicity of the antileukemic drug adaphostin has been attributed to its ability to localize in the mitochondrial membranes where it inhibits complex III resulting in the generation of ROS (22). Similarly to 11β, adaphostin accumulates to milimolar concentrations in the mitochondria; blocks cellular and mitochondrial respiration; perturbs mitochondrial inner membrane potential; and exhibits a cytotoxicity that can be ameliorated by co-treatment with antioxidants (22). However, not all compounds that generate oxidative stress interact with mitochondria directly. Compounds such as cisplatin (3), staurosporine (23) and the proteasome inhibitor bortezumib (24) are known to increase $\Delta\Psi m$ leading to increased ROS production, but in each case, the effect is apparently not due to a direct interaction with the mitochondria, but rather to a perturbation of the metabolic pathways involved in maintaining cellular redox homeostasis. In addition to its direct effect on the mitochondria, 11β also perturbs the cellular redox homeostasis as evidenced by the rapid decline in cellular NADPH levels (Fig. 3F). Whether this effect is due solely to the increased cellular ROS levels, or there is a different metabolic pathway affected by 11β, remains the object for further investigation.

Agents that induce oxidative stress have already been used to sensitize resistant cancer cells to alkylating drugs and radiation (25-27). There is also evidence that cancer cells are more sensitive to ROS induction than differentiated cells (2). Indeed, the generation of ROS and the concurrent depletion of antioxidant capacity can result in activation of stress-responsive genes leading to apoptosis or necrosis (2;28). One of the challenges of this therapeutic approach is matching both the pharmacokinetic and pharmacodynamic properties of different treatment protocols to enhance tumor response (29). The 11β compound represents a simplified approach by incorporating two mechanisms into a single molecule (Fig. 9) as 11β is both a DNA-alkylating compound (8) and a potent inducer of oxidative stress (current study). Furthermore, whereas alkylating agents such as chlorambucil have been found to induce only a transient oxidative stress response at high doses (30), 11β induces a sustained generation of ROS that may be more effective in sensitizing cells by antioxidant depletion. The sustained oxidative stress induced by 11β is likely due to its mitochondrial accumulation and specific ETC inhibition at complex I. Given the effectiveness of 11β against cancer cells both in cell culture (Fig. 1B) and in tumor xenografts (Fig. 8), understanding the detailed molecular mechanism of complex I inhibition remains an important stepping stone for pre-clinical development and warrants further investigation.

Continued interest in 11β as a potential anticancer drug stems from its ability to inhibit the growth of prostate tumors in xenograft animal models (7), with minimal side-effects on the animal host. We originally proposed that this anticancer activity is due to the ability of 11β-DNA adducts to bind the AR and increase toxicity by interfering with the DNA repair process as well as by antagonizing the expression of AR-regulated genes. In this report we demonstrate cytotoxic activity against another tumor cell line (HeLa), which lacks the AR, and characterize an additional mechanism of toxicity that involves mitochondrial ETC complex I inhibition and ROS generation. The combined actions of 11β in targeting both the mitochondrion and the nucleus (Fig. 9) distinguish it from existing anticancer drugs that either solely generate ROS (*i.e.*, quinones by redox cycling (31)) or primarily form DNA adducts (*i.e.*, simple aniline mustards). However, the fact that equimolar mixtures of chlorambucil and 11β-dim did not recreate the potent toxicity of 11β (Fig. 7) suggests that the interplay between the two mechanisms of toxicity is more complex and requires further investigation. Nevertheless, the concurrent ability to akylate DNA and induce ROS by perturbing mitochondrial function appears to be a useful paradigm for the design of broad-specificity antitumor compounds.

REFERENCES

1. Ruan, K., Song, G., and Ouyang, G. (2009) *J. Cell. Biochem* **107,** 1053-1062

2. Ozben, T. (2007) *J. Pharm. Sci.* **96,** 2181-2196

3. Nowak, G. (2002) *J Biol Chem* **277,** 43377-43388

4. Ravid, A., Rocker, D., Machlenkin, A., Rotem, C., Hochman, A., Kessler-Icekson, G., Liberman, U. A., and Koren, R. (1999) *Cancer Res* **59,** 862-867

5. Wallach-Dayan, S. B., Izbicki, G., Cohen, P. Y., Gerstl-Golan, R., Fine, A., and Breuer, R. (2006) *Am. J. Physiol. Lung Cell Mol. Physiol* **290,** L790-L796

6. Kapiszewska, M., Cierniak, A., Elas, M., and Lankoff, A. (2007) *Toxicol In Vitro* **21,** 1020-1030

7. Marquis, J. C., Hillier, S. M., Dinaut, A. N., Rodrigues, D., Mitra, K., Essigmann, J. M., and Croy, R. G. (2005) *Chem Biol* **12,** 779-787

8. Hillier, S. M., Marquis, J. C., Zayas, B., Wishnok, J. S., Liberman, R. G., Skipper, P. L., Tannenbaum, S. R., Essigmann, J. M., and Croy, R. G. (2006) *Mol Cancer Ther* **5,** 977-984

9. Cossarizza, A., Baccarani-Contri, M., Kalashnikova, G., and Franceschi, C. (1993) *Biochem. Biophys. Res. Commun* **197,** 40-45

10. Frezza, C., Cipolat, S., and Scorrano, L. (2007) *Nat. Protoc.* **2,** 287-295

11. Estornell, E., Fato, R., Pallotti, F., and Lenaz, G. (1993) *FEBS Lett.* **332,** 127-131

12. Nelson-Rees, W. A., Hunter, L., Darlington, G. J., and O'Brien, S. J. (1980) *Cytogenet Cell Genet* **27,** 216-231

13. Petronilli, V., Pietrobon, D., Zoratti, M., and Azzone, G. F. (1986) *Eur. J Biochem* **155,** 423-431

14. Ott, M., Gogvadze, V., Orrenius, S., and Zhivotovsky, B. (2007) *Apoptosis* **12,** 913-922

15. Hengartner, M. O. (2000) *Nature* **407,** 770-776

16. Jakubowski, W. and Bartosz, G. (2000) *Cell Biol. Int* **24,** 757-760

17. Robinson, K. M., Janes, M. S., Pehar, M., Monette, J. S., Ross, M. F., Hagen, T. M., Murphy, M. P., and Beckman, J. S. (2006) *Proc. Natl. Acad. Sci. U. S. A* **103,** 15038-15043

18. Murphy, M. P. (2009) *Biochem. J* **417,** 1-13

19. Murphy, M. P. (2008) *Biochim. Biophys. Acta* **1777,** 1028-1031

20. Weiss, M. J., Wong, J. R., Ha, C. S., Bleday, R., Salem, R. R., Steele, G. D., and Chen, L. B. (1987) *Proc. Natl. Acad. Sci. U. S. A* **84,** 5444-5448

21. Turrens, J. F. (2003) *J Physiol* **552,** 335-344

22. Le, S. B., Hailer, M. K., Buhrow, S., Wang, Q., Flatten, K., Pediaditakis, P., Bible, K. C., Lewis, L. D., Sausville, E. A., Pang, Y. P., Ames, M. M., Lemasters, J. J., Holmuhamedov, E. L., and Kaufmann, S. H. (2007) *J Biol Chem* **282,** 8860-8872

23. Poppe, M., Reimertz, C., Dussmann, H., Krohn, A. J., Luetjens, C. M., Bockelmann, D., Nieminen, A. L., Kogel, D., and Prehn, J. H. (2001) *J Neurosci.* **21,** 4551-4563

24. Ling, Y. H., Liebes, L., Zou, Y., and Perez-Soler, R. (2003) *J Biol Chem* **278,** 33714-33723

25. Fang, J., Seki, T., and Maeda, H. (2009) *Adv. Drug Deliv. Rev.* **61,** 290-302

26. Laurent, A., Nicco, C., Chereau, C., Goulvestre, C., Alexandre, J., Alves, A., Levy, E., Goldwasser, F., Panis, Y., Soubrane, O., Weill, B., and Batteux, F. (2005) *Cancer Res* **65,** 948-956

27. Nicco, C., Laurent, A., Chereau, C., Weill, B., and Batteux, F. (2005) *Biomed. Pharmacother.* **59,** 169-174

28. Mates, J. M. and Sanchez-Jimenez, F. M. (2000) *Int J Biochem Cell Biol* **32,** 157-170

29. Fang, J., Deng, D., Nakamura, H., Akuta, T., Qin, H., Iyer, A. K., Greish, K., and Maeda, H. (2008) *Int J Cancer* **122,** 1135-1144

30. Das, G. C., Bacsi, A., Shrivastav, M., Hazra, T. K., and Boldogh, I. (2006) *Mol Carcinog.* **45,** 635-647

31. Powis, G. (1989) *Free Radic. Biol. Med* **6,** 63-101

FOOTNOTES

*This research was supported by NIH grant RO1 CA077743 and Award Number DAMD17-98-1-8520 from the DOD PCRP.

[§]Present address: Molecular Insight Pharmaceuticals, Cambridge, MA 02142
[‡]Present address: Cancer and Stem Cell Biology Program, Duke-NUS Graduate Medical School, Singapore 169857

Supplementary information is available at the Journal of Biological Chemistry website.

The abbreviations used are: 11β, Carbamic acid, [3-[4-[bis(2-chloroethyl)amino]phenyl]propyl]-, 2-[[6-[(11.beta.,17.beta.)-17-hydroxy-3-oxoestra-4,9-dien-11-yl]hexyl]amino]ethyl ester, (CAS # 865070-37-7); 11β-dim, Carbamic acid, [3-[4-[bis(2-methoxyethyl)amino]phenyl]propyl]-, 2-[[6-[(11.beta.,17.beta.)-17-hydroxy-3-oxoestra-4,9-dien-11-yl]hexyl]amino]ethyl ester, (CAS # 865070-39-9); ROS, reactive oxygen species; H_2O_2, hydrogen peroxide; NAC, N-acetyl L-cysteine; CM-H_2DCFDA, 5-(and-6)-chloromethyl-2',7'-dichlorodihydrofluorescein diacetate; CM-DCFDA, 5-(and-6)-chloromethyl-2',7'-fluorescein diacetate; CTB, cell-titer blue; JC-1, 5,5',6,6'-tetrachloro-l,l',3,3'-tetraethylbenzimidazol-carbocyanine iodide; AR, androgen receptor; HBSS, Hanks' balanced salt solution; AMA, antimycin A; CMB, chlorambucil; EDO, 17β-hydroxy-estra-4(5),9(10)dien-3-one; STS, staurosporin; NBP, 4-(4-nitro-benzyl)-pyridine; ROT, rotenone; FCCP, 4-(trifluoromethoxy)phenylhydrazone; PARP, poly (ADPribose) polymerase; ETC, electron transport chain; FACS, fluorescence-activated cell sorting.

FIGURE LEGENDS

Fig. 1. Structures of compounds and their effects on HeLa cell viability and apoptosis. (A) The antitumor agent 11β is an aniline mustard linked to the steroid ligand estradiene-3-one (EDO). Similarly to chlorambucil (CMB), 11β contains the p-*N,N*-bis-(2-chloroethly)aminophenyl moiety capable of forming reactive aziridinium ions that produce covalent DNA adducts (DNA damage). The unreactive analog 11β-dim substitutes methoxy groups for chlorine atoms, which prevent formation of aziridinium ions and hence abolishes the ability to interact covalently with DNA. (B) Cell viability (estimated with the CTB assay) following 24 h treatment with 11β, 11β-dim, CMB or EDO. (C) Cell viability (assayed at 24 h) following treatments with the indicated concentrations of 11β for 3, 6, or 24 h. Cell viability was estimated using the CTB assay. The viable cell fraction was calculated relative to vehicle-treated controls. Data represent average ± standard deviation, $n = 3$. (D) Western blot analysis investigating the cleavage of PARP, caspase-9 and caspase-3 following treatment with 11β for 6 h. β-Actin is included as a loading control. Staurosporine (STS) is shown as a positive control.

Fig. 2. Cellular uptake of 11β and intracellular localization. (A) 11β distribution between the medium and HeLa cells, after 6 h exposure to 5 μM 11β. (B) Relative intracellular localization of 11β in HeLa cells exposed for 6 h to 5 μM 11β. Subcellular fractionation was performed as described in Materials and Methods. (C) The concentration of 11β (in pmol/μg protein) in the subcellular fractions from part B. Data represent mean ± standard deviation, $n = 3$.

Fig. 3. Effects of 11β compounds on ROS levels and markers of oxidative stress in HeLa cells. (A) Representative histograms of flow cytometry experiments demonstrating increased fluorescence intensity of CM-DCF (the oxidized form of CM-H_2DCFDA) following treatment with 3 μM or 5 μM 11β for 6 h. (B) Quantitative estimates of changes in mean fluorescence intensity of CM-DCF following 6 h treatments with 5 μM 11β , 10 μM 11β-dim, 10 μM estradien-3-one (EDO) or 10 μM chlorambucil (CMB) as measured by flow cytometry. Antimycin A (AMA), used at 1 μM is shown as a positive control. (C-F) Time course of the levels of ROS and markers of oxidative stress after exposure to 5 μM 11β. (C) Time-dependent changes in mean fluorescence intensity of CM-H_2DCFDA as measured by flow cytometry; (D) H_2O_2 concentration; (E) malonic dialdehyde (MDA) concentration; (F) total cellular NADPH concentration. Assays performed as described in Materials and Methods. Data represent mean ± standard deviation, $n = 3$. * $p<0.05$, ** $p<0.01$.

Fig. 4. The effect of antioxidants on the toxicity of 11β compounds in HeLa cells. (A) HeLa cells were treated with 5 μM 11β for 6 h in the presence of NAC (10 mM), vitamin E (100 μM) or vehicle (DMSO). Cells were then loaded with CM-H_2DCFDA and the mean fluorescence intensity determined by flow cytometry. (B) Cell viability following 24 h treatment with 11β alone or in the presence of NAC (10 mM) or vitamin E (100 μM). (C) Cell viability following 24 h treatment with 11β-dim alone or in the presence of NAC (10 mM), vitamin E (100 μM). Data represent average ± standard deviation, $n = 3$; * $p<0.05$, ** $p<0.01$.

Fig. 5. Effects of 11β on superoxide levels and ΔΨm in HeLa cells. (A) Cells were treated with DMSO (left panels) or 5 μM 11β for 6 h (right panels) then loaded with the mitochondrial $O_2^{\bullet-}$ indicator MitoSox Red and Hoechst 33342 and imaged by fluorescence microscopy. Top panels display enhanced mitochondrial $O_2^{\bullet-}$ production in 11β-treated cells. Middle panels show nuclear staining for reference. Bottom panels show merged images. Magnification is 100×. (B) Quantitative estimates of dose-dependent changes in mean fluorescence intensity of MitoSox Red following 6 h treatments with 11β as measured by flow cytometry. (C) 11β-induced changes in ΔΨm. Cells were treated with the indicated concentrations of 11β for 6 h in the absence or presence of NAC (10 mM) or Vitamin E (100 μM). The

cells were then loaded with JC-1 dye and the fluorescence measured by flow cytometry. Data represent mean ± standard deviation, $n = 3$, * $p < 0.05$, ** $p < 0.01$.

Fig. 6. Effects of 11β on cellular and mitochondrial respiration. (A) Cellular oxygen consumption was measured as described in Materials and Methods. HeLa cells were treated with 5 μM 11β or DMSO for 2 h, then oxygen consumption was measured in the presence of FCCP (1 nM), a mitochondrial ETC uncoupler. (B) Oxygen consumption in isolated rat liver mitochondria uncoupled with FCCP (1 nM). To test the electron flow through ETC via complexes I-III-IV, a glutamate/malate mix was used as a substrate. Rotenone (ROT), 1 μM was used as a control. To test the electron flow via complexes II-III-IV, succinate and rotenone (1 μM final) were used. In each case, oxygen consumption was determined in the presence of DMSO control, 11β or 11β-dim at the indicated concentrations. (C) Oxygen consumption in isolated rat liver mitochondria, using NADH as a substrate. The mitochondria were permeabilized to NADH by 3 freeze-thaw cycles. Rotenone (1 μM) was used as a control. (D) Complex I activity was measured in permeabilized mitochondria, by spectrophotometrically monitoring the disappearance of the NADH substrate. Decylubiquinone was used as the final electron acceptor. Rotenone (1 μM) was used as a positive control. Data represent average ± standard deviation, $n = 3$. (E) Production of H_2O_2 in isolated rat liver mitochondria following exposure to the 11β compounds. Mitochondria, charged with glutamate/malate, were exposed for 20 min at 37 °C to the indicated amounts of 11β, 11β-dim, or rotenone control (1 μM), in the presence or absence of 2000 U/mL of bovine liver catalase. The rate of H_2O_2 produced was then determined using the Amplex Red method. Data respresent average ± standard deviation, $n = 4$, * $p < 0.05$, ** $p < 0.01$.

Fig. 7. **Clonogenic survival of HeLa cells treated with 11β, 11β-dim, chlorambucil or 11β-dim/chlorambucil equimolar mixture.** Surviving fraction was determined by staining and counting colonies after 7 days. Data represent mean ± standard deviation, $n = 3$.

Fig. 8. Effect of 11β treatment on HeLa tumor xenografts. Mice bearing established HeLa tumors were dosed by daily injection with 30 mg/kg 11β or vehicle only. *Points*, mean tumor volume; *bars*, SD; *horizontal bars*, periods of dosing.

Fig. 9. The proposed mechanisms of toxicity. The substantial antitumor activity of 11β is proposed to be due to its ability to utilize two distinct mechanisms of toxicity: (i) DNA adduct formation and (ii) mitochondrial ROS production. Similarly to other nitrogen mustards, such as chlorambucil (top) 11β forms covalent DNA adducts (DNA damage). However, 11β is also a potent mitochondrial respiration inhibitor and oxidative stress inducer. The second mechanism of toxicity is recapitulated by 11β-dim (bottom), the dimethoxy derivative of 11β that cannot form DNA adducts, suggesting that the two mechanisms are distinct. The concurrent ability of 11β to damage DNA and induce mitochondrial ROS appears to be a useful paradigm for the design of broad-specificity antitumor agents.

FIGURE 1

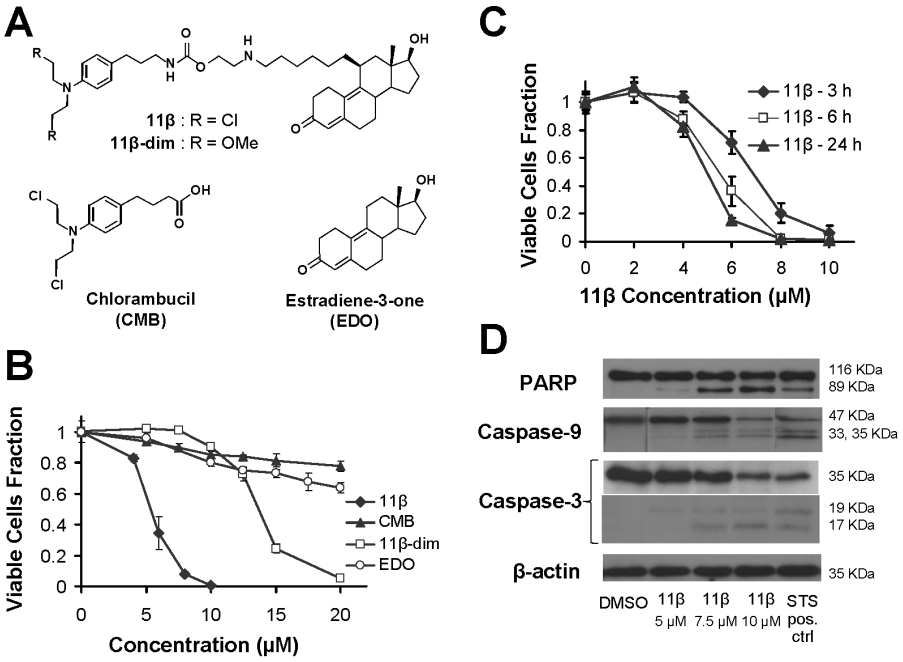
A
11β : R = Cl
11β-dim : R = OMe
Chlorambucil
(CMB)
Estradiene-3-one
(EDO)
B
Viable Cells Fraction
Concentration (μM)
11β
CMB
11β-dim
EDO
C
Viable Cells Fraction
11β Concentration (μM)
11β - 3 h
11β - 6 h
11β - 24 h
D
PARP
Caspase-9
Caspase-3
β-actin
116 KDa
89 KDa
47 KDa
33, 35 KDa
35 KDa
19 KDa
17 KDa
35 KDa
DMSO
11β 5 μM
11β 7.5 μM
11β 10 μM
STS pos. ctrl

FIGURE 2

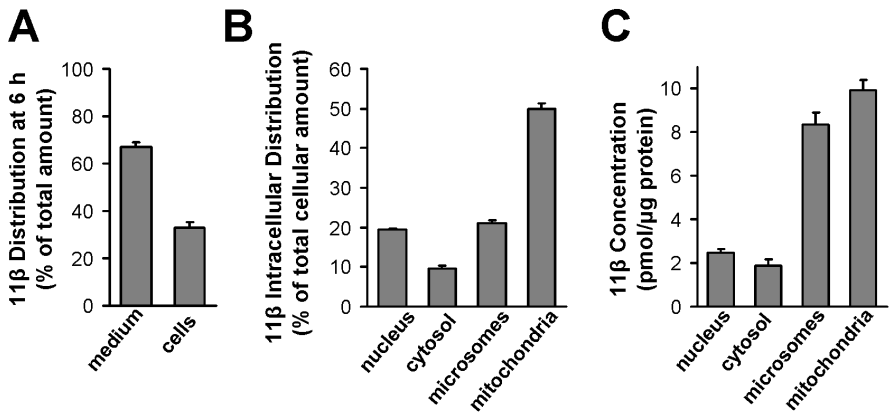
A
11β Distribution at 6 h (% of total amount)
100
80
60
40
20
0
medium
cells
B
11β Intracellular Distribution (% of total cellular amount)
60
50
40
30
20
10
0
nucleus
cytosol
microsomes
mitochondria
C
11β Concentration (pmol/µg protein)
10
8
6
4
2
0
nucleus
cytosol
microsomes
mitochondria

FIGURE 3

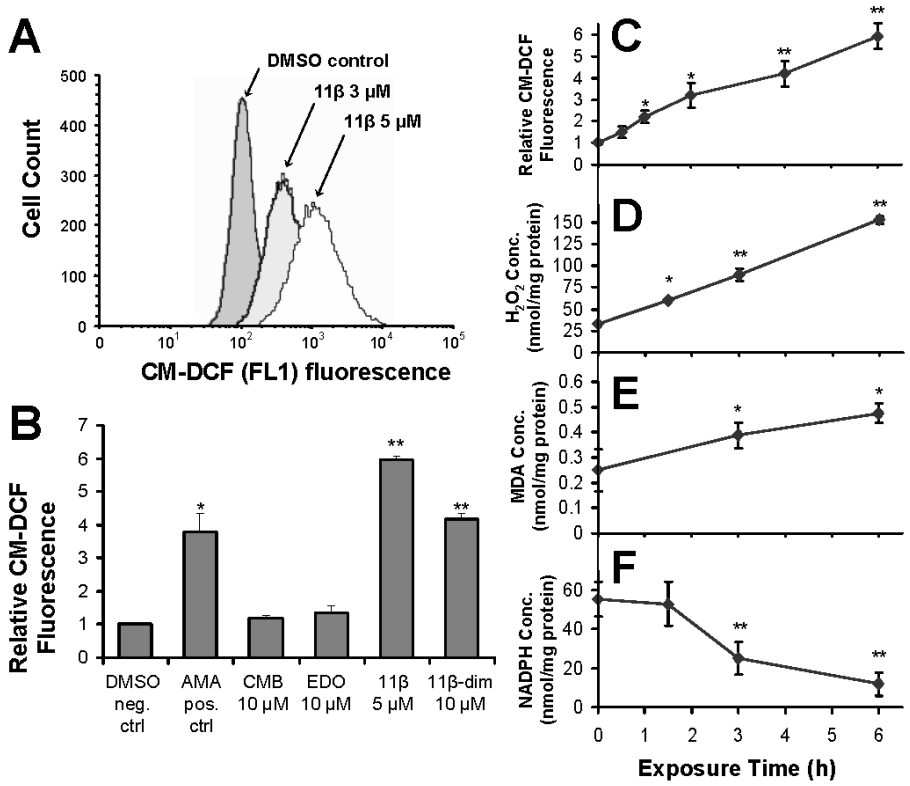
A
DMSO control
11β 3 μM
11β 5 μM
Cell Count
CM-DCF (FL1) fluorescence
B
Relative CM-DCF Fluorescence
DMSO neg. ctrl
AMA pos. ctrl
CMB 10 μM
EDO 10 μM
11β 5 μM
11β-dim 10 μM
C
Relative CM-DCF Fluorescence
D
H2O2 Conc. (nmol/mg protein)
E
MDA Conc. (nmol/mg protein)
F
NADPH Conc. (nmol/mg protein)
Exposure Time (h)

FIGURE 4

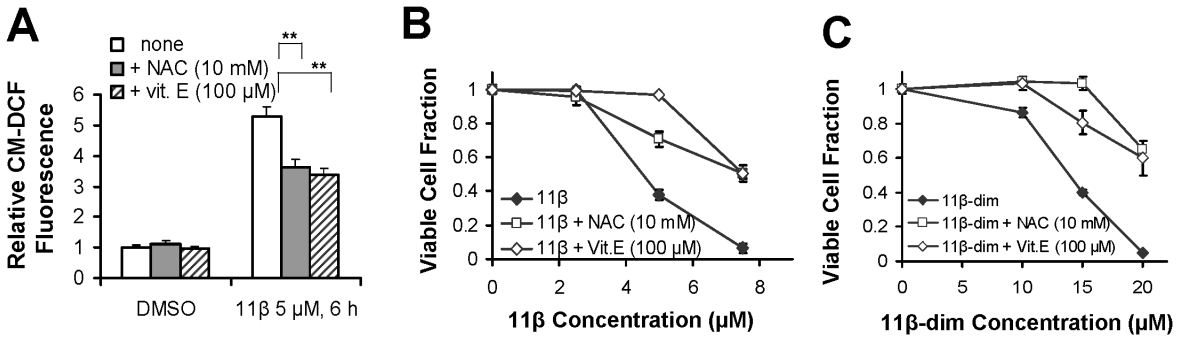
A
none
+ NAC (10 mM)
+ vit. E (100 µM)
**
**
Relative CM-DCF Fluorescence
0
1
2
3
4
5
6
DMSO
11β 5 µM, 6 h
B
Viable Cell Fraction
0
0.2
0.4
0.6
0.8
1
11β
11β + NAC (10 mM)
11β + Vit.E (100 µM)
0
2
4
6
8
11β Concentration (µM)
C
Viable Cell Fraction
0
0.2
0.4
0.6
0.8
1
11β-dim
11β-dim + NAC (10 mM)
11β-dim + Vit.E (100 µM)
0
5
10
15
20
11β-dim Concentration (µM)

FIGURE 5

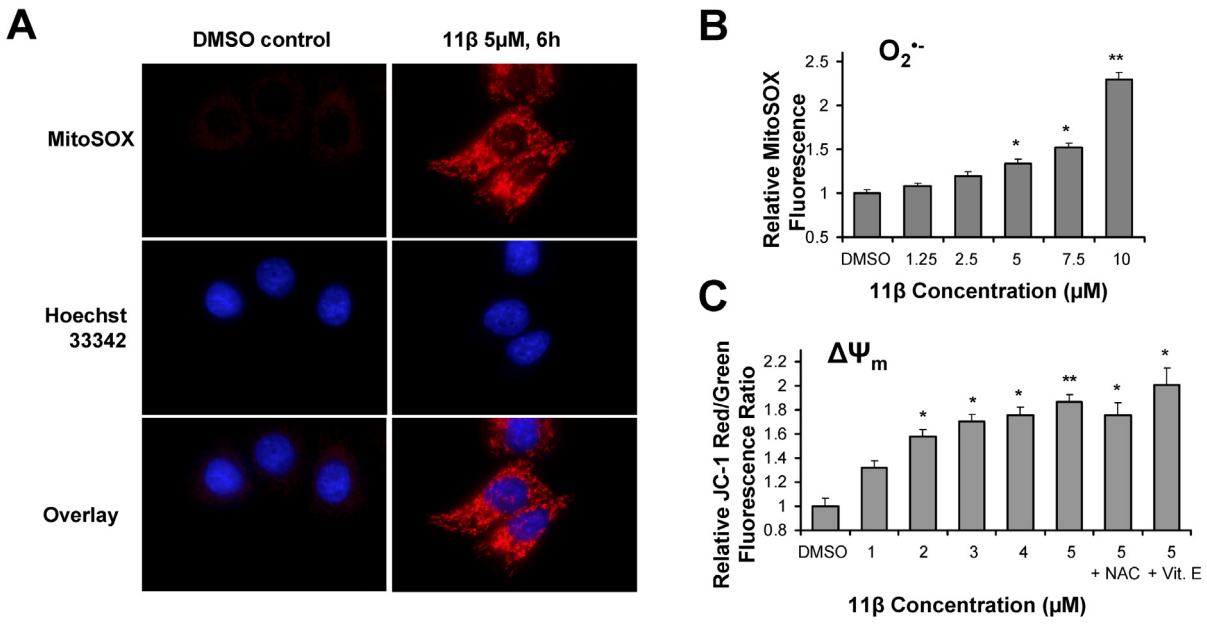
A
DMSO control
11β 5μM, 6h
MitoSOX
Hoechst 33342
Overlay
B
$O_2^{\bullet-}$
Relative MitoSOX Fluorescence
2.5
2
1.5
1
0.5
DMSO 1.25 2.5 5 7.5 10
11β Concentration (μM)
C
$\Delta\Psi_m$
Relative JC-1 Red/Green Fluorescence Ratio
2.2
2
1.8
1.6
1.4
1.2
1
0.8
DMSO 1 2 3 4 5 5 5
+ NAC + Vit. E
11β Concentration (μM)

FIGURE 6

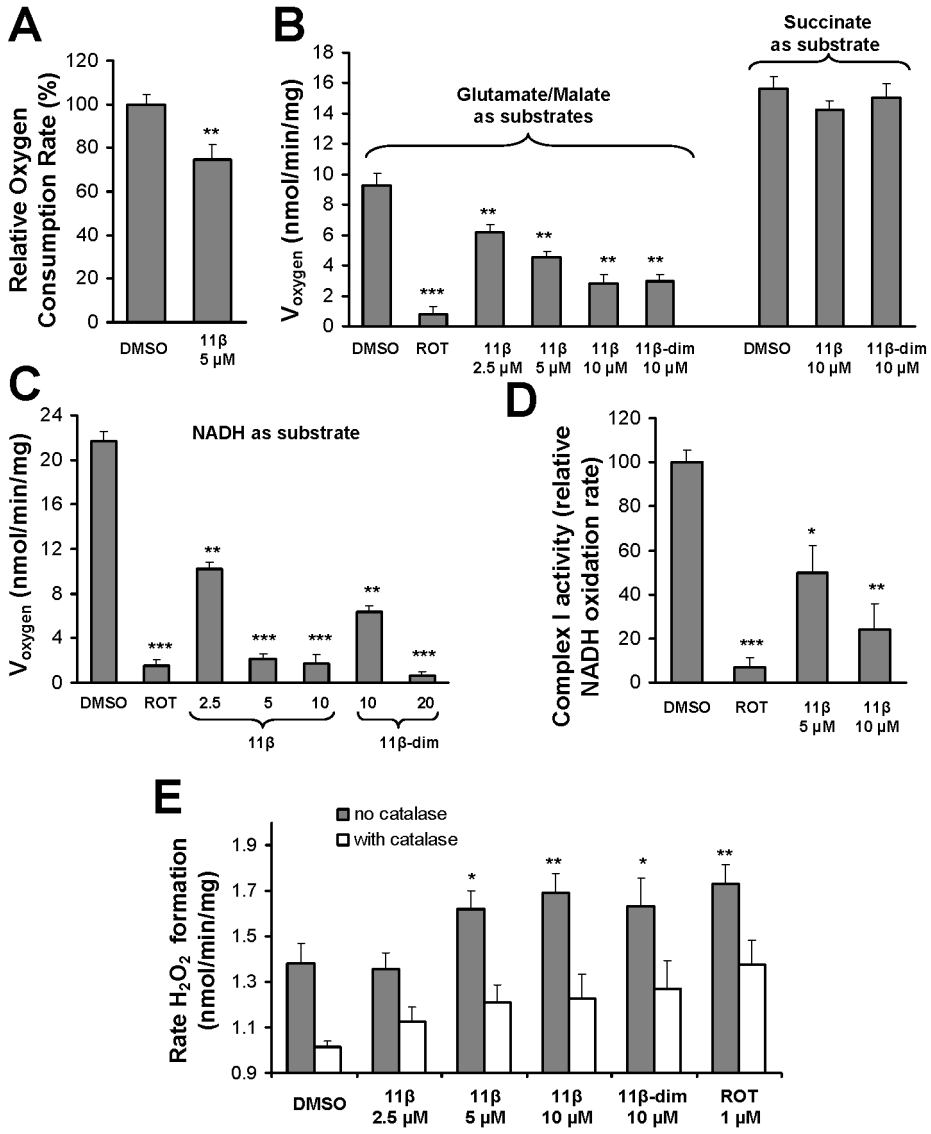
A
Relative Oxygen Consumption Rate (%)
DMSO
11β 5 μM
B
Succinate as substrate
Glutamate/Malate as substrates
Voxygen (nmol/min/mg)
DMSO
ROT
11β 2.5 μM
11β 5 μM
11β 10 μM
11β-dim 10 μM
DMSO
11β 10 μM
11β-dim 10 μM
C
NADH as substrate
Voxygen (nmol/min/mg)
DMSO
ROT
2.5
5
10
10
20
11β
11β-dim
D
Complex I activity (relative NADH oxidation rate)
DMSO
ROT
11β 5 μM
11β 10 μM
E
no catalase
with catalase
Rate H2O2 formation (nmol/min/mg)
DMSO
11β 2.5 μM
11β 5 μM
11β 10 μM
11β-dim 10 μM
ROT 1 μM

FIGURE 7

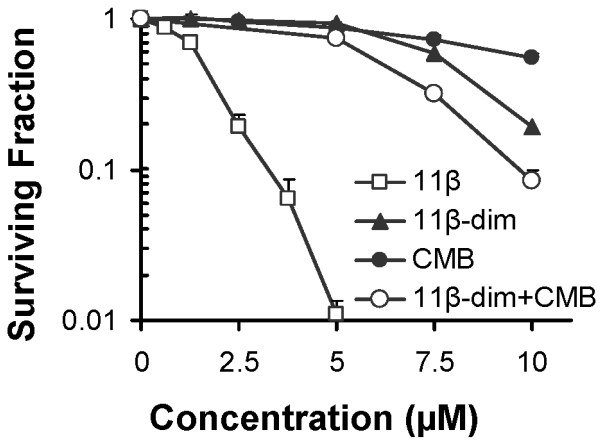
Surviving Fraction
1
0.1
0.01
0
2.5
5
7.5
10
Concentration (μM)
11β
11β-dim
CMB
11β-dim+CMB

FIGURE 8

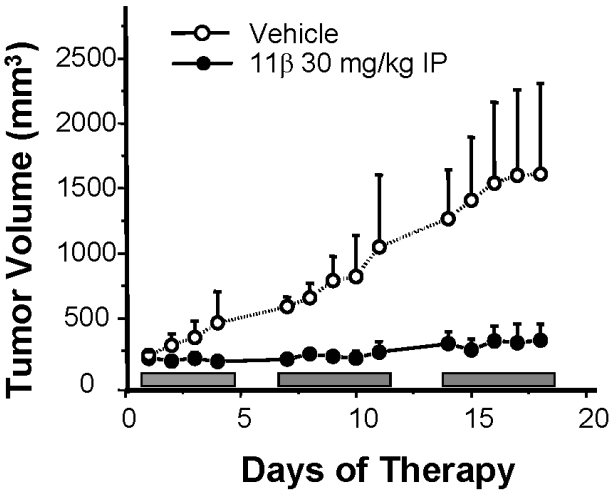
Vehicle
11β 30 mg/kg IP
Tumor Volume (mm³)
2500
2000
1500
1000
500
0
0
5
10
15
20
Days of Therapy

FIGURE 9